J. Fluid Mech. (1992), *vol.* 239, *pp.* 195–211
Printed in Great Britain

Wave properties of natural-convection boundary layers

By S. W. ARMFIELD† AND JOHN C. PATTERSON
Centre for Water Research, University of Western Australia, Australia 6009

(Received 20 December 1990 and in revised form 27 November 1991)

The thermal boundary layer on the wall of a side-heated cavity at early time is known to exhibit a complex travelling wave during growth to steady state and a similar feature is observed on isolated heated semi-infinite plates. Direct numerical solutions of the Navier–Stokes equations together with a linearized stability analysis are used to study the character of the flow at early time in detail. It is demonstrated that the cavity flow is essentially identical to the plate flow, and that for early time the flow is one-dimensional. Using the stability results it has been possible to accurately describe the form of the observed instability, as well as to reconcile a previously unexplained discrepancy in the speed of development of the flow.

1. Introduction

Natural convection in rectangular cavities with unequally heated sidewalls is a problem of fundamental interest to fluid mechanics and heat transfer, with many geophysical and industrial applications. In many cases the application of the side heating is unsteady in some sense, and the transient response of the system is important.

A specific problem which has been of considerable recent interest is that of an isothermal (at temperature T_m), stationary fluid in a square cavity. At time $t = 0$ the opposing vertical walls are instantaneously heated and cooled to $T_m \pm \frac{1}{2}\Delta T$. Briefly, the flow that evolves consists of narrow boundary layers on the vertical walls exiting from the downstream corners in heated and cooled intrusions. These intrusions fill the cavity, resulting in a nearly linear stratification in the core at steady state. A full description of the flow evolution to steady state is given in Patterson & Armfield (1990), following earlier papers based on experimental, numerical and scaling results by Patterson & Imberger (1980), Ivey (1984), Schladow, Patterson & Street (1989), and Schladow (1990).

In particular, during the transient phase of the flow two periods of instability are observed on the walls, one occurring at start up and the other when the wall boundary layer is first struck by the intrusion travelling across the cavity from the far side. This behaviour was first reported by Armfield (1989), Patterson (1989), and later in more detail by Schladow (1990) and Armfield & Patterson (1991). The instability takes the form of waves travelling in the flow direction, that is up the hot wall and down the cold wall, and has been likened in the papers cited above to similar waves observed on an isolated, instantaneously heated or cooled, semi-infinite vertical plate. Waves of a similar type have also been observed in air (Prandtl number = 0.71), by Paolucci (1990). In Schladow (1990) and Armfield & Patterson

† Current address: Department of Civil and Environmental Engineering, University of Western Australia, Australia 6009.

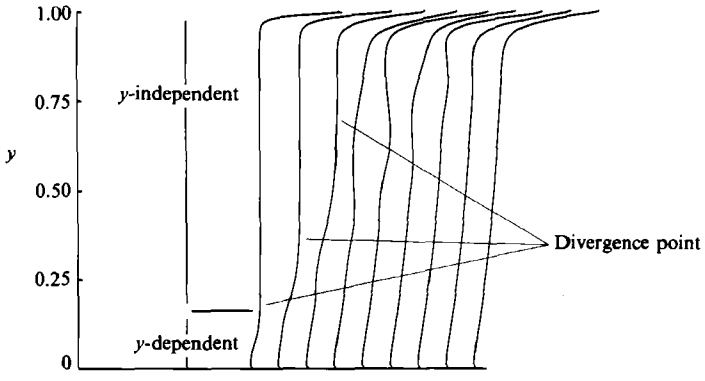

FIGURE 1. Offset vertical profiles of the temperature ($x = 8.3 \times 10^{-3}$) at a range of times, with the earliest time profile at the left.

(1991) it was suggested that at early times the development of the thermal boundary layers on the cavity walls was identical to that of the thermal boundary layer on such a plate. The present paper will focus on the stage during the development of the cavity flow when the thermal boundary layers on the walls are identical to those of the plate flow.

For simplicity, since the Boussinesq approximation is used and therefore the cavity flow is centro-symmetric, only the hot wall will be discussed. Physically the flow will not be centro-symmetric, owing to the nonlinear behaviour of density and viscosity with temperature, which is eliminated when the Boussinesq approximation is used. Comparison with experimental results indicates that the error associated with the assumption of centro-symmetry, for the Rayleigh numbers considered, is small. In the following, the origin of the coordinate system is at the base of the hot wall with the horizontal coordinate x positive in the interior of the cavity. The vertical coordinate y coincides with the cavity wall. The flow will be compared to that on a semi-infinite vertical plate with base located at the origin.

Previous studies of the development of the instantaneously heated plate flow give a general indication of its development as follows (for example, Goldstein & Briggs 1964; Brown & Riley 1973; Joshi & Gebhart 1987). Immediately following the start of heating, the y-dependence of the flow is contained in a singularity at the leading edge of the plate. The singularity is frequently referred to as the leading-edge point or leading-edge signal. Away from the leading edge the solution is entirely one-dimensional, with variation in the x-direction only. An analytic form for this one-dimensional solution is available. Subsequently, the singularity is advected up the plate with fluid that has been entrained at the leading edge. This introduces a y-variation into the flow and results in a divergence from the one-dimensional solution and the beginning of transition to steady state. If the temperature at a point has grown to be greater than the steady-state value by the time the leading-edge signal arrives, then the solution relaxes to the steady-state value from above, and a temperature overshoot is observed. Ingham (1985) considered the case of an impulsively heated plate in which the temperature on the plate varied as the power of the distance from the leading edge. Ingham's results indicated that when the power governing the variation was allowed to approach zero, that is the temperature on the plate approached a constant value, an oscillatory approach to steady state was observed; however, this was not identified as a travelling wave. It was also suggested that a discontinuous transition to the steady state could occur for the

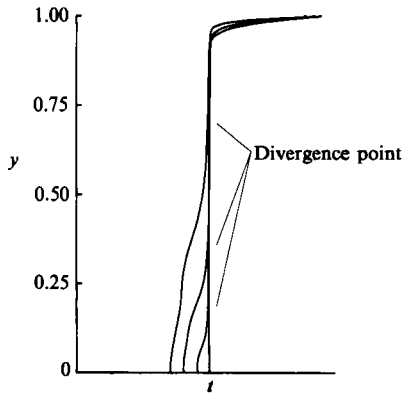

FIGURE 2. Vertical profiles of temperature from figure 1 overlaid to show the passage of the divergence point.

constant-temperature plate. Unfortunately Ingham was unable to obtain solutions for the constant-temperature plate and so these hypotheses could not be tested and it is possible that the appearance of a discontinuous transition could have resulted from the lack of diffusion in the boundary-layer equations used in the analysis.

This early part of the flow development may be readily seen in figures 1 and 2. In figure 1 vertical profiles of the temperature are presented at $x = 8.3 \times 10^{-3}$ of the cavity width in from the hot wall, at a range of times, with the greater time profiles offset to the right. It is seen in figure 1 that each of the three earliest time profiles consists of a region, near to $y = 0$, which varies with y, and a region far from $y = 0$ which is independent of y. These two regions are marked on the figure as y-dependent and y-independent for the first profile. In figure 2 the three earliest time profiles are shown with the y-independent regions overlaid on top of each other and on the zero-time solution, which is a vertical line. The rapid y-variation at the top of the profiles is due to the effect of the cavity ceiling and is not considered in the present discussion. The point separating the y-dependent and y-independent regions is marked on the figures as the divergence point and is seen to travel upward for the first three profiles of figure 1. By the time of the fourth profile the divergence point has reached the top of the cavity and the entire profile is y-dependent. The passage of the divergence point and the separation of the profiles into y-dependent and y-independent regimes is also clearly seen in figure 2. It is suggested that the divergence point marked on these figures and discussed in the present paper corresponds to the earliest arrival of information from the leading edge and thus is a graphical representation of the leading-edge signal hypothesized in the papers cited above.

After the passage of the divergence point, and the overshoot if it occurs, a series of waves is observed to travel up the hot wall, for sufficiently high Rayleigh numbers, where the Rayleigh number Ra is defined below. In general the overshoot and the travelling waves have been grouped together and referred to as a sinusoidal oscillation (Schladow 1990). The travelling waves increase in amplitude in the positive y-direction while the amplitude of the overshoot varies only slightly. When observed at a fixed y-location the signal is observed to decay and the effect is thus transitory. For higher Rayleigh numbers this decay does not occur (Joshi & Gebhart 1987). Indeed Joshi & Gebhart suggest that at sufficiently high Ra values the travelling waves are associated with a transition to turbulence.

As the divergence point, the overshoot and the travelling waves are passing up the plate, the base flow is itself evolving. Thus the character of the flow near to $y = 0$ will

be different to that far from $y = 0$, at the time of the passage of the effects described above. The boundary layer near to $y = 0$ at the time of passage will be narrower with a smaller maximum velocity than that for larger y values. The flow for small y will be stable while that further away will be unstable, indicating that at some critical height there will be a transition from stable to unstable regimes. A Rayleigh number based on this height is termed the critical Rayleigh number. In §4 it is shown that the critical Rayleigh number obtained for the evolving flow corresponds well to that obtained for the fully developed flow. The similarity of the critical Rayleigh numbers for the evolving and the fully developed flow indicates that at the time the leading-edge point passes a y-location the flow at that location has a stability character approximately the same as the fully developed flow has at that location.

Stability analysis of fully developed boundary layers on heated vertical plates indicates that, at Rayleigh numbers below that at which transition to turbulence occurs but above the critical value, the boundary layer will act to selectively amplify a small band of wavenumbers (Gebhart & Mahajan 1982). For this range of Ra values the boundary layer is therefore acting as a bandpass filter. This is consistent with the observation of travelling waves in the boundary layer of the cavity flow (Schladow 1990; Armfield & Patterson 1991). Gill & Davey (1969), in a stability analysis of flow between infinite differentially heated vertical plates, suggested that travelling wave modes could exist with a velocity, with respect to the fixed coordinate system defined above, greater than the maximum flow velocity.

In the present paper we utilize the results of a direct simulation of the cavity flow, as described in §2, in a stability analysis to study in detail the early phase of the cavity boundary layer. For validation, the numerical solution is briefly compared with experimental results. Further, numerical solutions for the semi-infinite plate flow have been generated and are used to verify the assumption that the cavity-flow thermal boundary layer is, at early time, well approximated by the plate flow. Comparison is also made between the plate flow, the cavity flow and the one-dimensional analytic solution of the boundary-layer equations to confirm that the early part of the flow in both cases is indeed one-dimensional.

Using these results it has been possible to identify the cause of a previously unexplained discrepancy between the maximum flow velocity and the velocity of the divergence point dividing the flow into y-independent and y-dependent regimes. It has also been possible to verify the prediction of Gill & Davey (1969) that waves travelling at greater than the maximum flow velocity may be present. Further, analysis of the numerical results allows a clear delineation between the temperature overshoot and the subsequent travelling waves.

The remainder of the paper is as follows. Section 2 briefly describes the numerical method used to obtain the full solution of the Navier–Stokes equations for the cavity and the plate flow. Additionally, in §2 the method used in the stability analysis together with the one-dimensional solution of the boundary-layer equations is given. The results of the stability analysis are presented in §3 for Prandtl numbers (defined below) $Pr = 7.5$, 13 and 18, all at a Rayleigh of approximately 6×10^8. These Prandtl numbers were chosen to match the available experimental results (Jeeveraj & Patterson 1992). Section 4 contains the discussion while the conclusion are given in §5.

2. Method

2.1. *Numerical method*

The governing equations for both the cavity and the plate flow are the usual Navier–Stokes and the conservation of heat equations. The Boussinesq assumption allows the incompressible form of the equations to be used which are then written in conservative, non-dimensional form as

$$U_t+(UU)_x+(VU)_y=-P_x+(U_{xx}+U_{yy}), \tag{1}$$

$$V_t+(UV)_x+(VV)_y=-P_y+(V_{xx}+V_{yy})+\frac{Ra}{Pr}(T-T_m), \tag{2}$$

$$U_x+V_y=0, \tag{3}$$

$$T_t+(UT)_x+(VT)_y=\frac{1}{Pr}(T_{xx}+T_{yy}), \tag{4}$$

where subscripts denote partial differentiation, U is the velocity component in the x-direction, V the velocity component in the y-direction, T the temperature and T_m the mean temperature. The Rayleigh number and Prandtl number are defined as,

$$Ra=g\beta H^3(\Delta T)/\nu\kappa, \qquad Pr=\nu/\kappa,$$

where g is the acceleration due to gravity, β the coefficient of thermal expansion, H the height of the cavity, ν the kinematic viscosity and κ the thermal diffusivity. In the above equations, and in all results presented, length is non-dimensionalized by H, $T-T_m$ by ΔT, the total temperature variation, and time by H^2/ν.

For the cavity flow the top and bottom are insulated and all boundaries are non-slip. Initially the fluid is at rest and isothermal ($T=T_m$) and at $t=0$ the sidewalls are heated and cooled impulsively to $T_m\pm\frac{1}{2}\Delta T$. The semi-infinite plate is modelled by a long plate of length H, in initially isothermal and stationary fluid. At $t=0$, the plate, is impulsively heated to $T_m+\frac{1}{2}\Delta T$. In both cases a mesh that concentrates points in the region of the wall is required to resolve the boundary-layer lengthscales. For the cavity, the mesh used locates a point one thousandth of the cavity width in from the wall, expands at a rate of 10% until the edge of the thermal boundary layer is reached, and is then held constant until the far boundary layer is reached. The resultant mesh is shown in figure 3. The same computational domain and mesh are used for the plate flow, with the hot wall of the cavity corresponding to the plate, and the boundaries corresponding to the lid and the cold wall of the cavity, having zero normal gradient in velocity and temperature. The boundary corresponding to the floor also has zero normal gradient in the velocity while the temperature there is set directly to zero. The time step used is sufficiently short to resolve the shortest timescales of the boundary-layer start-up.

The cases dealt with here correspond to the simulations undertaken in Patterson & Armfield (1990) and Armfield & Patterson (1991). Thus the cavity modelled is 24 cm square, and the resulting mesh is 80×80. The required time step is $\sim 1.0\times10^{-5}$, for the values of Ra used.

Full details of the numerical scheme are given in the papers referred to above and in Armfield (1991). Briefly, the equations are discretized on a non-staggered mesh, but using a method of obtaining the pressure field and satisfying continuity similar

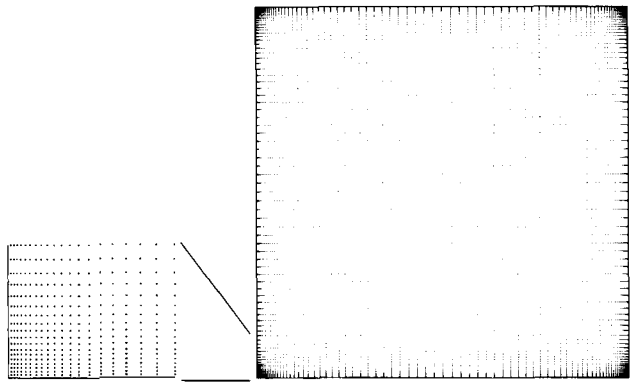

FIGURE 3. Mesh used for computation with bottom-left corner enlarged.

to the usual SIMPLE scheme on a staggered mesh (Armfield 1991). The convective terms are differenced by a third-order upwind scheme, and time integration is carried out by a Crank–Nicolson predictor–corrector method.

In both the plate and cavity flows the velocity and temperature fields in the boundary layer are of interest and, as will be shown below, these are essentially one-dimensional for times prior to the passage of the first group of travelling waves.

2.2. *Stability analysis*

The stability of the flow in the boundary layer is determined by the usual linear stability analysis of the one-dimensional numerical solution of the Navier–Stokes equations, and the one-dimensional analytical solution given by Goldstein & Briggs (1964). The Goldstein & Briggs solution of the boundary-layer equations on the impulsively heated plate is

$$V = \frac{4g\beta t\Delta TH}{2\nu(1-Pr)}[\mathrm{i}^2\,\mathrm{erfc}\,\eta - \mathrm{i}^2\,\mathrm{erfc}\,(\eta/Pr^{\frac{1}{2}})], \tag{5}$$

$$T = \tfrac{1}{2}\mathrm{erfc}\,\eta, \tag{6}$$

with $\eta = x/(4\kappa t)^{\frac{1}{2}}$ and $\mathrm{i}^n\,\mathrm{erfc}$ the *nth* integral of the complementary error function. The horizontal velocity is zero, and as can be seen there is no y-dependence in T or V.

To examine the stability of this flow, an infinitesimal perturbation is added to each of the components, and the perturbed fields put into the Navier–Stokes equations. The resulting equations are linearized in the usual way to provide a set of eigenvalue equations for the perturbations. Thus, if the perturbations to the stream function and temperature are described by ψ and τ respectively, where

$$\psi = \mathrm{Re}\,(\psi(x)\exp[\mathrm{i}\alpha(y-ct)]), \tag{7}$$

$$\tau = \mathrm{Re}\,(\tau(x)\exp[\mathrm{i}\alpha(y-ct)]), \tag{8}$$

and Re (f) denotes the real part of f, α is real and c is complex, then substitution into the appropriate form of the Navier–Stokes equations yields, on ignoring products of the perturbations, the stability equations (Gill & Davey 1969)

$$\psi^{\mathrm{iv}} - 2\alpha^2\psi'' + \alpha^4\psi - \mathrm{i}\alpha[(V-c)(\psi''-\alpha^2\psi) - V''\psi] + \tau' Ra/Pr = 0, \tag{9}$$

$$\tau'' - \alpha^2\tau - \mathrm{i}\alpha Pr[(V-c)\tau - T'\psi] = 0. \tag{10}$$

with boundary conditions

$$\tau(0) = \psi(0) = \psi'(0) = 0 \quad \text{for} \quad x = 0, \tag{11}$$

$$\tau(x), \psi(x), \psi'(x) \to 0 \quad \text{as} \quad x \to \infty. \tag{12}$$

For both the numerical and analytic solutions, the large-x boundary condition is applied at half the cavity width, $x = 0.5$. The validity of applying the large-x boundary condition at $x = 0.5$ was tested by applying the boundary condition for the analytic solution at locations up to $x = 5.0$, with no discernible difference in the results being observed.

Equations (9) and (10) are eigenvalue equations for α and c. The equations are discretized using a second-order shooting method and then integrated using the orthonormalization technique of Davey (1973). Calculation of the eigenvalues is then reduced to obtaining the values of Ra, Pr, α and c for which the determinant of a 3×3 matrix is zero. A simplex minimization procedure is used to search for these zeros. For a given wavenumber α, the amplification is αc_i, where c_i is the imaginary component of c, while c_r, the real component of c, is the wave velocity. Thus calculation of the eigenvalues yields, for a given Ra–Pr pair, a relationship between the wavenumber, the wave speed and the amplification.

3. Results

Full numerical solutions of the cavity and plate problems have been obtained for the Ra–Pr pairs: (i) $Ra = 6 \times 10^8$, $Pr = 7.5$; (ii) $Ra = 5.4 \times 10^8$, $Pr = 13$; (iii) $Ra = 6.2 \times 10^8$, $Pr = 18$. These have been compared with the one-dimensional analytical solution given in (5) and (6), and with the experimental results given in Jeeveraj & Patterson (1991).

The result of these comparisons for case (i), in the form of temperature time series taken in the boundary layer at mid-height ($y = 0.5, x = 1.25 \times 10^{-2}$) is shown in figure 4. Several features are apparent: first, for $t < 3.5 \times 10^{-4}$, the two numerical results coincide with the one-dimensional analytical solution; second, following the separation of the signals, the numerical solutions reach a peak value, and subsequently undergo a decaying oscillation; third, the plate and cavity solutions are virtually identical until the oscillations begin, and then differ only slightly in the amplitude of the oscillations and in the steady state; fourth, the initial experimental response appears to lag the numerical result by approximately 1.0×10^{-4}, while the subsequent oscillatory behaviour, although approximately in phase with the numerical result, has a somewhat smaller amplitude and longer period.

The timing difference between the experimental and numerical results for the cavity flow has been discussed in Patterson & Armfield (1990) and Armfield & Patterson (1991), and is most likely the result of the experiment being at a lower Ra than expected. A comparison of the experimental result and a numerical result obtained at a Rayleigh number of 4.8×10^8, 80% of that given above, is shown in figure 5. The arrival time and phase of the oscillation are now well represented, supporting the hypothesis that the experimental Rayleigh number is lower than expected. These comparisons, together with the extended comparisons in Patterson & Armfield (1990), confirm that the numerical method is accurately modelling the physics of the cavity flow. The lower than expected experimental Rayleigh number is most likely the result of boundary layers forming, despite vigorous stirring, in the water baths used to heat and cool the cavity sidewalls.

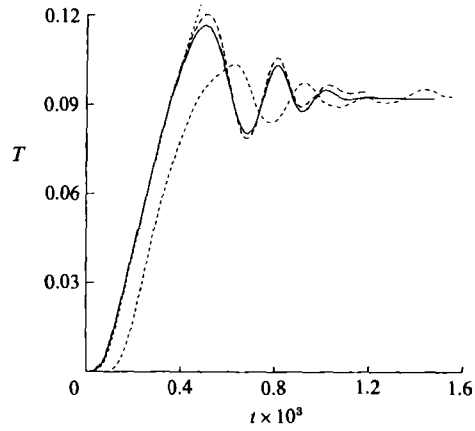

FIGURE 4. Temperature time series for case (i) $Ra = 6 \times 10^8$, $Pr = 7.5$, at $x = 1.25 \times 10^{-2}$, $y = 0.5$ for the numerical cavity flow (solid line), the numerical plate flow (long dashed line), the experimental cavity flow (short dashed line) and the analytic one-dimensional solution (dotted line).

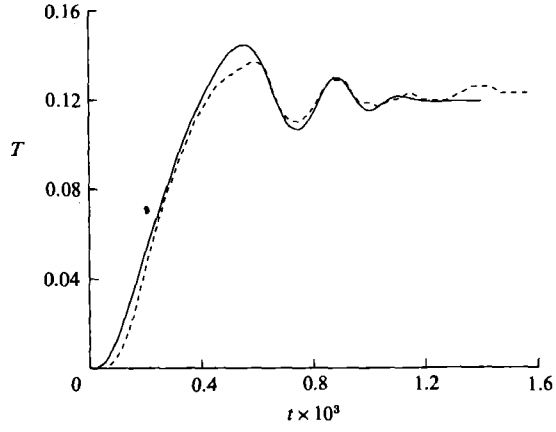

FIGURE 5. Temperature time series at $x = 1.25 \times 10^{-2}$, $y = 0.5$ for the numerical cavity flow (solid line) at $Ra = 4.8 \times 10^8$ and the experimental cavity flow (dashed line).

The similarity between the plate and cavity results for the times shown confirms that the plate flow is good model for the cavity boundary-layer flow, at least for the initial part of the development. This means that the conclusions in the literature pertaining to the waves travelling on the boundary layer of the plate are also relevant to the cavity, and vice versa. Finally, the coincidence of the one-dimensional solution with the full numerical solution for the early part of the flow indicates that, for the early period of the flow development, the one-dimensional assumption is valid.

Figure 6 shows a comparison of the numerically calculated velocity and temperature profiles for the plate and cavity flow with the corresponding one-dimensional analytical solutions, at $y = 0.5$ and $t = 2.8 \times 10^{-4}$. Clearly, the agreement within the region of interest is excellent. In the interior, however, the cavity flow has a velocity reversal, which is not present in the plate flow or the one-dimensional solution. These comparisons were made at other vertical and horizontal positions (excluding the upper end of the cavity) with, for all cases, the same conclusions. For

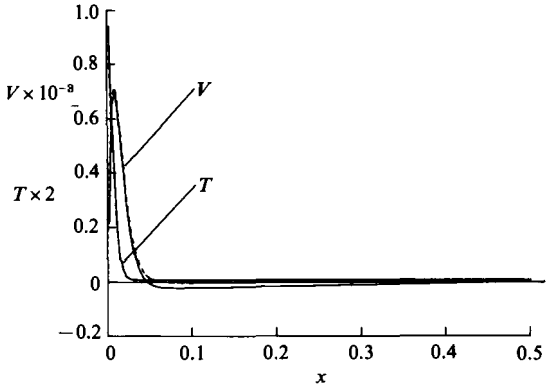

FIGURE 6. Temperature and velocity profiles at $y = 0.05$ and $t = 2.8 \times 10^{-4}$ for the numerical cavity flow (solid line), the numerical plate flow (dashed line) and the analytic one-dimensional solution (dotted line).

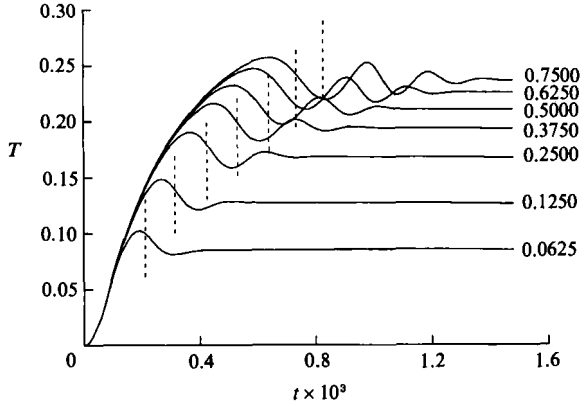

FIGURE 7. Temperature time series at $x = 8.3 \times 10^{-3}$ and the seven y-locations shown on the figure for the numerical cavity flow. The vertical dashed lines mark the arrival time of the maximum flow velocity point at each y-location.

conciseness these are not shown. The occurrence of the velocity reversal in the cavity only is due to at least some of the fluid ejected into the intrusion falling back down into the cavity and being re-entrained. This feature is associated with the cavity ceiling and thus is not expected in the semi-infinite plate flow.

Figure 7 shows the temperature time series from the numerical solution of the cavity flow, for case (i), at $x = 8.3 \times 10^{-3}$ and at a number of different y-locations. Figure 8 shows the $y = 0.75$ result, with the overshoot and the travelling waves marked. Using the results presented in figure 7 it is possible to examine some aspects of the nature of the oscillation formed by the combination of the overshoot and the travelling waves, which have been briefly described in the introduction. From figure 7 it is evident that the amplitude of the overshoot varies only slightly with increasing y, while the period increases considerably, more than doubling over the range shown. Conversely the amplitude of the travelling waves increase significantly over the range shown, while there is negligible variation in the period. The overshoot and the travelling waves are therefore distinct features.

The time at which the curve for a given y-location diverges from that for a larger y corresponds to the arrival of the divergence point and subsequent divergence from

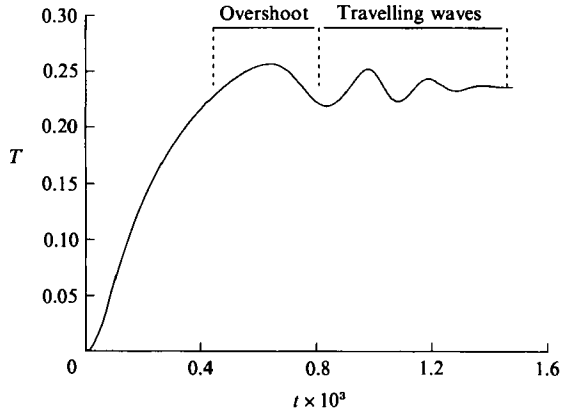

FIGURE 8. Temperature time series at $x = 8.3 \times 10^{-3}$ and $y = 0.75$ for the numerical cavity flow with the temperature overshoot and the travelling waves marked.

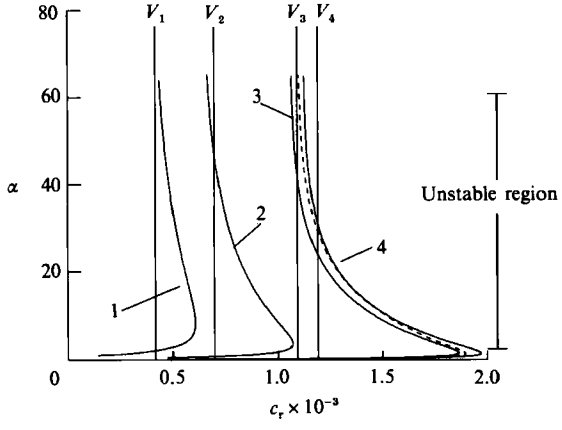

FIGURE 9. Wavenumber α versus wave speed c_r obtained at $t = 4.7 \times 10^{-4}$ using the one-dimensional base flow (dashed line) and at $t = 1.8 \times 10^{-4}$, 2.3×10^{-4}, 4.0×10^{-4} and 4.7×10^{-4} using the numerical cavity base flow (solid lines). Maximum flow velocities are marked on the plot as V_1, V_2, V_3 and V_4, corresponding to the solution at 1.8×10^{-4}, 2.3×10^{-4}, 4.0×10^{-4} and 4.7×10^{-4} respectively.

the simple one-dimensional solution. From figure 7, this point of divergence has a velocity of 2.2×10^3 as it passes the mid-height location $y = 0.5$. Similarly, the velocities of the travelling waves may be calculated from the figure; for the first wave (the second peak in the curve), the velocity at mid-height is 1.4×10^3, while that of the second wave, although difficult to determine exactly, is approximately the same. The overshoot (the first peak in the curve) has a velocity between that of the divergence and the first wave. The period of the travelling waves is 2.1×10^{-4}, while the amplification factor at the $y = 0.5$ location is 4.4×10^3.

The arrival time of a fluid parcel which has travelled from the leading edge at the maximum flow velocity, obtained by integrating the numerically calculated vertical velocity, is also marked on the plot. This is consistently later than the divergence time. Correspondingly, the resulting maximum flow velocity at mid-height is 1.2×10^3, substantially slower than the divergence point velocity of 2.2×10^3.

These results indicate that there are three characteristic velocities associated with the development of the boundary layer. In order of increasing magnitude they are:

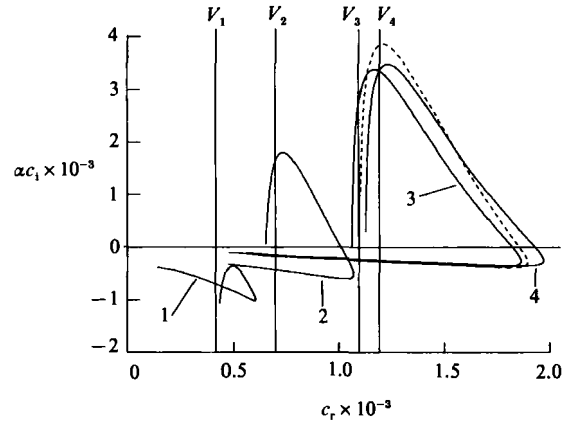

FIGURE 10. Amplification αc_i versus wave speed c_r obtained at $t = 4.7 \times 10^{-4}$ using the one-dimensional base flow (dashed line) and at $t = 1.8 \times 10^{-4}$, 2.3×10^{-4}, 4.0×10^{-4} and 4.7×10^{-4} using the numerical cavity base flow (solid lines). Maximum flow velocities are marked on the plot as V_1, V_2, V_3 and V_4 corresponding to the solution at 1.8×10^{-4}, 2.3×10^{-4}, 4.0×10^{-4} and 4.7×10^{-4} respectively.

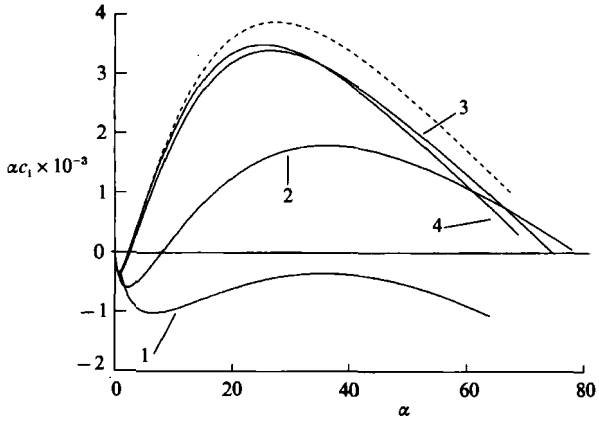

FIGURE 11. Amplification αc_i versus wavenumber α obtained at $t = 4.7 \times 10^{-4}$ using the one-dimensional base flow (dashed line) and at $t = 1.8 \times 10^{-4}$, 2.3×10^{-4}, 4.0×10^{-4} and 4.7×10^{-4} using the numerical cavity base flow (solid lines).

the maximum flow velocity, the travelling wave velocity and the divergence point velocity. These velocities will subsequently be denoted as v_m, v_w, and v_d, respectively.

3.1. *Stability analysis results*

The linearized stability analysis allows the character of the travelling waves in the boundary layer to be studied in more detail. The solution of the stability equations for any *Ra–Pr* pair using the numerically calculated or analytical vertical velocity and temperature profiles yields eigenvalues of α, c_r, and c_i, for which a solution exists. Figure 9 shows the resulting wavenumber α, for case (i), plotted against the wave speed c_r at four times for the numerically calculated solution, and at a single time for the one-dimensional analytical solution. Figure 10 shows the amplification αc_i plotted against the wave speed and figure 11 shows the amplification as a function of wavenumber. The time chosen for the comparison of the analytical and numerical results ($t = 4.7 \times 10^{-4}$) coincides with the passage of the divergence point at the mid-

height location. In all figures, the analytical and numerical results are very similar, again confirming the one-dimensional nature of the numerical result. In figures 9 and 10, the maximum flow velocities at each time are also shown as vertical lines. The results at $t = 4 \times 10^{-4}$ and 4.7×10^{-4} are presented to demonstrate that a small variation in the base flow leads to a small variation in the stability results, and thus the stability analysis itself is stable. This is important in the context of the present flow because the base flow is evolving as the travelling waves are passing up the wall.

Subsequent discussion will consider the stability results obtained using the numerical base flow solution, although the analytic base flow solution could have been obtained and used at the other times and would have yielded similar estimates for the stability characteristics.

Consider first the $t = 4.7 \times 10^{-4}$ result. From figure 11, a range of wavenumbers is amplified by the flow. This range is marked on figure 9. Clearly, much of this range has a wave speed greater than the maximum flow velocity, consistent with the observation that the maximum flow velocity is the smallest of the three characteristic velocities. The peak amplification occurs for a wavenumber of 24 (figure 11). The corresponding wave velocity, from figure 9, is 1.2×10^3, the corresponding period is 2.1×10^{-4} and the predicted amplification is 3.6×10^3. These compare with the estimates from figure 7 of 1.4×10^3, 2.1×10^{-4} and 4.5×10^3 for the travelling waves observed in the numerical results. Further, the peak signal velocity predicted by the stability analysis is 2.0×10^3; this corresponds to the velocity of the divergence from the one-dimensional flow, estimated from figure 7 as 2.2×10^3. Clearly the characteristics of the peak amplification wavenumber component obtained from the stability analysis accurately represent the observed features of the travelling wave, obtained from the numerical results given in figure 7.

Also shown in figures 9–11 are the results of the stability analysis for earlier times. Of interest here is that, although the general form of the relationship between the three parameters is similar, the wave speed and amplification are significantly reduced at earlier times. In particular, at $t = 1.8 \times 10^{-4}$, all wavenumbers are decaying in amplitude. Early time corresponds to the region of the thermal boundary layer close to the leading edge at the time of passage of the travelling wave disturbance; thus the figures show that in the first part of the flow the travelling waves are decaying in amplitude for all wavenumbers. At a particular time the amplification becomes positive at a specific wavenumber, corresponding to a critical distance from the leading edge. As the disturbance travels further up the wall, the range of amplified wavenumbers increases. However, only those waves subject to sufficient amplification will be readily visible. Thus the observed travelling waves are those with near to peak amplification as has been shown above.

The same analysis has also been performed for cases (ii) and (iii) above ($Pr = 13$ and 18). In these cases, there are minor changes in Ra, and the primary change is in the value of Pr, as compared to the Ra–Pr values in case (i). These pairs were determined by the available experimental data (Jeevaraj & Patterson 1991). In both cases (ii) and (iii), the same procedures were followed and a good agreement between the analytic solution, the numerical cavity flow, the numerical plate flow and the experimental results was obtained. Similarly the v_m, v_w and v_d obtained from the stability analysis accurately predicted those obtained directly from the numerical solution. In general, the results are consistent with those for case (i), and the details are not shown here. The wavenumber, wave speed, and amplification plots were of the same form as figures 9–11.

These results are summarized in table 1, which shows the results for all cases. Both

Flow	Method	v_m	v_w	v_d	p(s)
$Pr = 7.5$	Stability	1.2×10^3	1.2×10^3	2.0×10^3	2.1×10^{-4}
	Simulation	1.2×10^3	1.4×10^3	2.2×10^3	2.1×10^{-4}
$Pr = 13$	Stability	6.4×10^2	7.0×10^2	1.1×10^3	3.0×10^{-4}
	Simulation	6.4×10^2	8.0×10^2	1.1×10^3	3.2×10^{-4}
$Pr = 18$	Stability	7.1×10^2	7.5×10^2	1.2×10^3	2.8×10^{-4}
	Simulation	7.1×10^2	7.2×10^2	1.3×10^3	3.4×10^{-4}

TABLE 1. Comparison of v_m, v_w, v_d and p (the period) for the three flows

the velocities and wavelengths obtained from the full simulations and from the stability analysis are included; clearly the stability estimates match very well. Further, the ordering of the three characteristic velocities is the same for all three Prandtl numbers, with the wave velocity of order 10% greater than the maximum flow velocity, while the velocity of the divergence point is of order 70% greater.

4. Discussion

The results presented above indicate that the early part of the development of the thermal boundary layer on the wall in the side-heated cavity is a close approximation to the thermal boundary layer on an isolated heated semi-infinite plate, for Prandtl and Rayleigh numbers similar to those considered. This is because the local cavity flow, at the y-locations shown, is not significantly influenced by the cavity lid or the far wall. At considerably lower Rayleigh numbers, or higher Prandtl numbers, the similarity between the two flows would no longer hold, as the boundary-layer scale is then proportional to the cavity scale and the flow is strongly influenced by the cavity lid and far wall within the time-scale of the boundary-layer development. For instance, using the scaling given by Patterson & Imberger (1990), the viscous boundary-layer thickness is obtained as $\delta_\nu \sim Pr^{\frac{1}{2}}/Ra^{\frac{1}{4}}$ suggesting a minimum Rayleigh number at $Pr = 7.5$, for similarity between the cavity and plate flows, of $Ra \sim 1000$. Similarly, for later times than those considered here, the cavity flow will diverge considerably from the plate flow as the influence of the upper boundary and the intrusion from the far wall is felt.

It is well known that the plate flow develops initially as a one-dimensional solution to the temperature and vertical momentum equations, the analytic form of which is given in equations (5) and (6). Because of this similarity the cavity boundary layer is also well approximated by the one-dimensional solution. Thus, as is expected, the stability analysis of the one-dimensional analytic solution yields a good approximation to that of the numerical solution.

The important features of the early development of the flow that have been considered are the passage of the divergence point separating the one-dimensional y-independent solution and the later y-dependent solution, the overshoot in the temperature solution and the subsequent travelling waves. Owing to the similarity of the cavity and plate flows it is evident that the conclusions here are, by implication, applicable to the plate flow. Likewise, it is evident that the conclusions obtained by others for the plate flow are applicable here.

A detailed examination of the numerical simulation has indicated that the divergence point dividing the y-dependent and y-independent parts of the solution travels up the wall at a velocity considerably greater than the maximum flow

velocity. It was initially hypothesized by Goldstein & Briggs (1964), and later by Brown & Riley (1973), that this divergence point would travel at the maximum flow velocity. More recent experimental and numerical studies (Joshi & Gebhart 1987; Schladow 1990) have also reported that the divergence point travels considerably faster than the maximum flow velocity. Joshi & Gebhart in particular noticed that for sufficiently high Rayleigh numbers the flow would uniformly and instantaneously diverge from the one-dimensional solution. This suggested that the divergence point had an infinite velocity and was most likely the result of the amplification of local disturbances. This is clearly not the case in the present flow in which the divergence point travels at a finite, measurable velocity up the wall. Schladow (1990) also observed this velocity discrepancy at a similar Ra values, but without further discussion.

Previous stability studies have indicated that travelling waves may exist with a velocity greater than the maximum flow velocity (Gill & Davey 1969). However, such studies were primarily concerned with obtaining constant amplification curves in wavenumber/Grashof number space. Thus, although the existence of disturbance velocities greater than the maximum flow velocity was predicted by the stability analysis, the link to experimental or numerical data, or to the passage of the divergence point, was not made.

The presentation of the stability results in the form of trajectories in wavenumber/wave speed, amplification/wave speed, and amplification/wavenumber space in the present study clearly demonstrates the existence of a peak disturbance velocity considerably greater than the maximum flow velocity. Comparison of the peak disturbance predicted by the stability analysis with the divergence velocity measured from the results of the simulation, in table 1, shows very good agreement in all cases, and thus the discrepancy between the divergence-point velocity and the maximum flow velocity observed in the current study and by previous researchers is explained.

Brown & Riley (1973) suggested that a singularity originating at the leading edge of the plate (referred to as the leading-edge point) travelled up the wall at the maximum flow velocity. They also suggested that it was the arrival of this point that triggered the divergence of the full solution from the purely one-dimensional solution. Thus the effect of their leading-edge point corresponds to that of the divergence point discussed in this paper; however, it is clear from the above results that the divergence point travels faster than the maximum flow velocity and additionally does not possess a singular character. Brown & Riley used as the basis for the analysis the usual boundary-layer equations with no streamwise diffusion which, if present, would remove the singular nature of the leading-edge point. Further, even without the effect of diffusion, the dispersive nature of the flow demonstrated by the stability results would act to transform the singularity.

As a result of the present analysis it is seen that the singularity generated at the leading edge $y = 0$, at $t = 0$ is the source of the observed travelling waves as well as of the divergence point. The singularity itself can be considered to consist of an infinite sum of discrete wavenumber components. Once the flow starts, each of the wavenumber components will start to travel up the wall at the velocity predicted by the dispersion relation in figure 9. The velocity of the fastest component will correspond to that of the divergence point. The slower travelling components of the singularity will follow the divergence point up the wall. A small band of wavenumbers will gain energy from the base flow once they pass a critical height at which initially a single wavenumber component transits to the unstable regime. As the waves

continue up the wall more energy passes into the component that was first to transit into the unstable regime, and ultimately this component becomes visible with a measurable amplification rate, giving rise to the observed travelling waves. Higher up the wall additional wavenumber components could be expected to become visible as they transit into an unstable regime and receive energy from the base flow. It is primarily the peaked nature of the amplification curve, together with the fact that once a component transits to an unstable regime it remains unstable, that gives the flow its filtering effect where a single wavenumber is initially selectively amplified and thus becomes clearly visible. As the leading edge produces only one singularity, at start-up, and as the velocity of the high-wavenumber components asymptotes to a constant velocity of approximately the maximum flow velocity, the signal is transient.

Goldstein & Briggs (1964) suggested that, in some cases, the temperature signal would overshoot its steady-state value in the initial development of the flow, and that the final relaxation to steady state would be from above rather than, as might be expected, from below. This hypothesis was based on a comparison of the rate of development of the one-dimensional thermal boundary layer and the maximum flow velocity, and included the assumption that the divergence point would travel at the maximum flow velocity. Thus, if the thermal boundary layer had grown to greater than its steady-state value by the time the divergence point had arrived, then an overshoot would be observed.

The oscillating signal observed here, and experimentally by Patterson & Armfield (1990) and Jeeveraj & Patterson (1992), is more complex than a simple overshoot. The signal is a combination of the overshoot predicted by Goldstein & Briggs and the travelling waves predicted by the stability analysis and discussed above. Thus the later part of the signal is formed by travelling waves consisting of those wavenumbers with near peak amplification. However, as was observed in §3 the overshoot, the initial peak in the signal, has a different character to the remainder of the signal. It is clearly present in the trace at $y = 0.0625$ and does not increase significantly in amplitude while increasing considerably in period with increasing y, the reverse of the travelling wave. This behaviour is not predicted by the stability analysis, indicating that the initial peak is not a travelling wave of the same form as the later peaks.

Thus the early development of the flow, up to and including the passage of the travelling waves, is based on the three characteristic velocities: the maximum flow velocity, the velocity of the maximum amplified wavenumber and the velocity of the divergence point. This behaviour is reflected in the shape of the amplification/wave speed plot with, approximately, the maximum flow velocity correspondingly to the right angle, the travelling wave velocity corresponding to the peak and the divergence velocity corresponding to the leading angle.

Using the early time stability results it is possible to obtain the location on the wall at which a single wavenumber component of the leading-edge singularity will first transit to an unstable regime. This may then be used to calculate approximately the critical Rayleigh number for which transition from stable to unstable flow occurs, for the $Pr = 7.5$ case, in the following way. Interpolation on figures 9 or 10 indicates that the flow passes through the neutral (zero amplification) surface at approximately 1.9×10^{-4}, with the maximum amplification available changing sign at a single wavenumber. Using figure 7 this time corresponds to the full development of the boundary layer at location $y \sim 0.166$, at which point the local Rayleigh number based on the y-value, will be 2.7×10^6. Gebhart & Mahajan (1982) present constant-

amplification surfaces for $Pr = 6.7$ in wavenumber/Grashof number space for fully developed flow on a heated vertical plate with constant flux boundary condition. Their results are presented in terms of a modified flux Grashof number G^* and indicate that transition occurs at $G^* = 20$. Using the relation $Gr \sim (G^*)^4$, where Gr is the Grashof number for the isothermal plate and $Ra = GrPr$, gives a predicted critical Rayleigh number of 1×10^6, based on the total temperature variation in the boundary layer. In the present context, with the Rayleigh number based on the total temperature variation in the cavity, this equals 2×10^6. Clearly both methods indicate transition occurring at approximately the same point.

5. Conclusions

A comparison of experimental, numerical and analytical results indicates that the early part of the development of the cavity convection flow for a range of Prandtl numbers can be accurately simulated by the numerical scheme described in §2. Comparisons of the simulation with experimental data for later times have been presented in Patterson & Armfield (1990) and demonstrate that accurate prediction is also obtained for the full development of the cavity flow. Additionally it has been shown that the thermal boundary layer on the wall for the cavity flow is approximately one-dimensional and that, at least until after the passage of the travelling wave instability, the flow is essentially that of an isolated heated semi-infinite plate. It has also been demonstrated that a good estimate for the stability characteristics of the cavity flow can be obtained from the analytic one-dimensional solution.

The discrepancy between the velocity of the divergence point and the maximum flow velocity is due to the existence of a peak disturbance velocity greater than the maximum flow velocity. Stability analysis predicts this discrepancy and accurately gives the divergence-point velocity.

The oscillation following the divergence of the full solution from the one-dimensional is a combination of temperature overshoot and the travelling wave modes that amplify in the y-direction. The initial peak in the oscillation is the temperature overshoot that occurs in the manner predicted by Goldstein & Briggs (1964), followed by the travelling waves, with only those most strongly amplified, that is those with wavenumbers near the peak of the amplification plot, being visible. These travel slower than the divergence point and thus the wavelength of the overshoot increases in the direction of travel.

The observed behaviour of the flow is thus explained by reference to the results of the stability analysis. In particular the flow features are characterized by three velocities: the maximum flow velocity, the maximum amplified wavenumber velocity and the peak disturbance (divergence point) velocity.

This research was supported by the Australian Research Council in the form of a National Research Fellowship and by grant A48615453, and by the Australian Water Research Advisory Council. The authors wish to thank Jorg Imberger, John Taylor, Song Ping Zhu and Geoff Schladow for their useful comments.

REFERENCES

ARMFIELD, S. W. 1989 Direct simulation of unsteady natural convection in a cavity. *Proc. Intl Symp. on Computational Fluid Dynamics, Nagoya*, pp. 305–310. North-Holland.

ARMFIELD, S. W. 1991 Finite difference solutions of the Navier–Stokes equations on staggered and non-staggered grids. *Computers Fluids* **20**, 1–17.

ARMFIELD, S. W. & PATTERSON, J. C. 1991 Direct simulation of wave interactions in unsteady natural convection in a cavity. *Intl J. Heat Mass Transfer* **34**, 929–940.

BROWN, S. N. & RILEY, N. 1973 Flow past a suddenly heated vertical plate. *J. Fluid Mech.* **59**, 225–237.

DAVEY, A. 1973 A simple numerical method for solving Orr–Sommerfeld problems. *Q. J. Mech. Appl. Maths* **24**, 401–410.

GEBHART, B. & MAHAJAN, R. L. 1982 Instability and transition in buoyancy induced flows. *Adv. Appl. Mech.* **18**, 231–315.

GILL, A. E. & DAVEY, A. 1969 Instabilities of a buoyancy driven system. *J. Fluid Mech.* **35**, 775–798.

GOLDSTEIN, R. J. & BRIGGS, D. G. 1964 Transient free convection about vertical plates and circular cylinders. *Trans. ASME* C: *J. Heat Transfer* **86**, 490–500.

INGHAM, D. 1985 Flow past a suddenly heated vertical plate. *Proc. R. Soc. Lond.* A **402**, 109–134.

IVEY, G. 1984 Experiments on transient natural convection in a cavity. *J. Fluid Mech.* **144**, 389–401.

JEEVERAJ, C. & PATTERSON, J. C. 1992 Experimental study of transient natural convection of glycerol- water mixtures in a side heated cavity. *Intl J. Heat Mass Transfer* (in press).

JOSHI, Y. & GEBHART, B. 1987 Transition of vertical natural convection flows in water. *J. Fluid Mech.* **179**, 407–438.

PAOLUCCI, S. 1989 Direct numerical simulation of two-dimensional turbulent natural convection in an enclosed cavity. *J. Fluid Mech.* **201**, 379–410.

PATTERSON, J. C. 1989 Experiments in unsteady natural convection. *Proc. Fourth Australasian Conf. on Heat and Mass Transfer*, Christchurch, pp. 299–306.

PATTERSON, J. C. & ARMFIELD, S. W. 1990 Transient features of natural convection in a cavity. *J. Fluid Mech.* **219**, 469–497.

PATTERSON, J. C. & IMBERGER, J. 1980 Unsteady natural convection in a rectangular cavity. *J. Fluid Mech.* **100**, 65–86.

SCHLADOW, S. G. 1990 Oscillatory motion in a side heated cavity. *J. Fluid Mech.* **213**, 589–610.

SCHLADOW, S. G., PATTERSON, J. C. & STREET, R. L. 1989 Transient flow in a side-heated cavity at high Rayleigh number. *J. Fluid Mech.* **200**, 121–148.